Author/s:
Xiong, Z;Chen, S;Zhao, P;Cho, Y;Odunmbaku, GO;Zheng, Y;Jones, DJ;Yang, C;Sun, K

Title:
Phase Transition Modulation and Defect Suppression in Perovskite Solar Cells Enabled by a Self-Sacrificed Template

Date:
2021-09-01

Citation:
Xiong, Z., Chen, S., Zhao, P., Cho, Y., Odunmbaku, G. O., Zheng, Y., Jones, D. J., Yang, C. & Sun, K. (2021). Phase Transition Modulation and Defect Suppression in Perovskite Solar Cells Enabled by a Self-Sacrificed Template. Solar Rrl, 5 (9), https://doi.org/10.1002/solr.202100448.

**Article type: Communication**

# Title: Phase Transition Modulation and Defects Suppression in Perovskite Solar Cells Enabled by a Self-sacrificed Template

*Zhuang Xiong*[a], *Shanshan Chen*[b], *Pengjun Zhao*[c], *Yongjoon Cho*[d], *George Omololu Odunmbaku*[a], *Yujie Zheng*[b], *David J. Jones*[c], *Changduk Yang*[d], *Kuan Sun*[a,*]

Zhuang Xiong, George Omololu Odunmbaku, Prof. Kuan Sun
[a] MOE Key Laboratory of Low-grade Energy Utilization Technologies and Systems, School of Energy & Power Engineering, Chongqing University, Chongqing 400044, China
E-mail: kuan.sun@cqu.edu.cn
Shanshan Chen, Yujie Zheng
[b] State Key Laboratory of Power Transmission Equipment & System Security and New Technology, School of Energy & Power Engineering, Chongqing University, Chongqing 400044, China
Pengjun Zhao, David J. Jones
[c] School of Chemistry, Bio21 Institute, The University of Melbourne, 30 Flemington Road, Parkville, Victoria 3010, Australia
Yongjoon Cho, Changduk Yang
[d] Department of Energy Engineering, School of Energy and Chemical Engineering, Perovtronics Research Center, Low Dimensional Carbon Materials Center, Ulsan National Institute of Science and Technology (UNIST), 50 UNIST-gil, Ulju-gun, Ulsan 44919, South Korea

Keywords: perovskite solar cells, self-sacrificed template, crystal growth, deep-level defects, non-radiative recombination.

Abstract: Tunable crystal growth offering highly aligned perovskite crystallites with suppressed deep-level defects is vital for efficient charge transport, which in turn significantly influences the power conversion efficiency (PCE) of perovskite solar cells (PSCs). In this study, a 'Precursor to Perovskite-like template to Perovskite' (PPP) growth strategy is developed, by using either MAAc or GuaCl precursor to induce a sacrificial thermal-unstable perovskite-like template for $(FAPbI_3)_x(MAPbI_3)_y$ perovskite growth. The self-sacrificed intermediate template induces the formation of highly aligned perovskite crystals with greatly enhanced film crystallinity and suppresses deep-level defect formation. Furthermore, it is proved that the MAAc or GuaCl is completely evaporated during the high temperature annealing process. The reduction in defect densities and non-radiative recombination enhances both carrier lifetime and charge dynamics, yielding impressive PCE of 22.3% and 22.8% with high open-circuit voltage ($V_{OC}$) of 1.16 V and incredible fill factor (FF) of 81.5% and 79.4% for MAAc and GuaCl based devices, respectively. These results suggest that formation of the thermal-unstable perovskite-like sacrificial template is a promising strategy to restrain the deep-level defects in perovskite films towards the attainment of highly efficient, and stable large-scaled PSCs as well as other perovskite-based electronics.

## 1. Introduction

Due to low formation energy, point defects are the most common defect types observed in organic-inorganic hybrid halide perovskites.[1] These point defects are typically suppressed by surface passivation approaches, especially by the introduction of supplementary halide anions.[2] However, deep-level point defects such as interstitials or anti-sites, whereby the formation depends on non-stoichiometric supply of the halide ions and unfavorable perovskite crystal growth

dynamics, cannot be suppressed by the surface passivation approach mentioned above.[3] At present, a common practice for reducing the deep-level defects in perovskite relies on control over the crystal growth kinetics. For example, the $PbI_2$-dimethylsulfoxide (DMSO) complex reported by Seok et al. can slow down the crystallization process, thus resulting in highly crystalline formamidinium lead iodide ($FAPbI_3$).[4] Nevertheless, using DMSO as the mediator may induce the formation of $[(Pb_3I_8)_n]^{2n-}$, which is an I-deficient intermediate that is charge-balanced by FA or methylamine (MA) cations.[3b, 5] Later on, acetate (Ac) anion additives were proposed due to its similar ionic radius to the iodide anion.[6] Ultra-smooth and pinhole-free perovskite film can be achieved by substitution of $PbI_2$ with PbAc as the lead source, leading to enhanced charge extraction.[7] Interface modification of $MAPbI_3$ perovskite with CsAc shows enhanced carrier kinetics and high fill factor (FF).[8] Recent studies show that dense and pinhole-free perovskite films with high reproducibility can be prepared without an anti-solvent, when a methylammonium acetate (MAAc) molten salt is adopted as the solvent in one step fabrication process.[9] Even though the anion substitution approach improves the perovskite crystal formation, it unfortunately limits the photovoltaic performance, which are always lower than 22%. In addition, the cation-deficient intermediate phase can further lead to the formation of a hexagonal non-perovskite phase, rather than a perovskite phase.[3b]

In this work, we demonstrate that a 'Precursor to Perovskite-like template to Perovskite' (PPP) growth strategy, by using the thermal-unstable perovskite-like template, can facilitate the growth of high-quality perovskite crystals. This strategy was achieved by incorporating MAAc or guanidine chloride (GuaCl) to $PbI_2$ precursor in a two-step perovskite formation process. During the evolution of the thermal-unstable perovskite-like intermediate template, the crystallization of both $PbI_2$

precursor layer and perovskite layer becomes more regular, giving rise to highly aligned crystal growth with reduced recombination centers. As a result, non-radiative recombination is reduced and charge transport is enhanced. The resultant MAAc-based and GuaCl-based devices with 1.3 M $PbI_2$ and 1.5 M $PbI_2$ exhibit superior power conversion efficiency (PCE) of 22.3% and 22.8% with dramatically enhanced FF of 81.5% and 79.4% compared to that of control devices (PCE=20.1% and 21.2%, FF=76.4% and 76.2%), respectively. Our approach exploits a 'precursor to perovskite-like self-sacrificed intermediate template to perovskite' growth strategy to stabilize the α-phase of $FAPbI_3$, and successfully hinders the formation of deep-level defects. This facile method provides an effective alternative to control the perovskite crystal growth that is vital to the development of perovskite-based electronic devices.

## 2. Results and discussion

The device configuration employed in this work is ITO/$SnO_2$/$(FAPbI_3)_x(MAPbI_3)_y$/2,2′,7,7′-tetrakis(N,Ndi-p-methoxyphenylamine)-9,9′-spirobifluorene (Spiro-OMeTAD)/$MoO_3$/Ag, as shown in **Figure 1a**. The MAAc-containing perovskite is grown by first introducing 3 vol% MAAc into the 1.3 M $PbI_2$ precursor solution to form a MAAc-$PbI_2$ film, followed by depositing organic halide compounds and thermal annealing. The detailed preparation process of perovskite layers and devices is provided in Experimental Section. As shown in **Figure 1b**, the control devices without MAAc exhibit a maximum PCE of 20.1% with an open circuit voltage ($V_{OC}$) of 1.12 V, a short-circuit current density ($J_{SC}$) of 23.5 $mAcm^{-2}$, and a FF of 76.4%. The use of MAAc additive offers a significantly enhanced FF value of 81.5%, along with an increased $V_{OC}$ of 1.16 V, yielding a boost in PCE to 22.3%. The simultaneous increase in $V_{OC}$ and FF parameters implies that the MAAc effectively reduces defect densities. **Figure 1c** displays the

monochromatic incident photon-to-electron conversion efficiency (IPCE) of both devices. The blue shift in peak positions, which is also observed in absorption spectra in **Figure S1**, and the drastic enhancement at 700 to 800 nm are related to the enhanced distribution of the $PbI_2$.[10] The integrated current densities are 22.1 $mAcm^{-2}$ and 22.5 $mAcm^{-2}$ for the control and MAAc-assisted device, respectively. The slightly increased integrated $J_{SC}$ value in MAAc-assisted device might be ascribed to the enhanced absorbance in perovskite layer (**Figure S1**). Moreover, the statistical distributions of performance for the control and MAAc-assisted devices confirm that the MAAc additive leads to highly reproducible photovoltaic performance (**Figure 1d**).

To gain insight into the effect of MAAc additive on the crystal packing and orientation of $PbI_2$ film, grazing incidence wide angle X-ray scattering (GIWAXS) measurement is carried out. As shown in **Figure 2a, b**, the neat $PbI_2$ film exhibits a more diffused (001) ring, implying the $PbI_2$ crystallites are randomly oriented in the film. In contrast, a sharp and discrete (001) spot along $q_z$ direction is observed for the $PbI_2$ mixed with MAAc, suggesting the formation of a vertically oriented crystalline $PbI_2$ film. This result is further confirmed by the intensity azimuthal pole figure of (001) diffractions of $PbI_2$ films in **Figure 2c**. Larger percentage of the (001) diffraction signals is located in the narrow azimuthal angle range between 80° and 90° for the MAAc-$PbI_2$ sample. In addition, the $PbI_2$ film with MAAc additive shows additional diffraction peaks at 14.2°, 24.4° and 24.7° in X-ray diffraction (XRD) pattern after annealing at 60℃ for over 5 min (**Figure 2d, e**). These additional peaks are assigned to (110), (112) and (202) crystal planes of a tetragonal perovskite-like phase.[11] In addition, the XPS measurement further prove the interaction between $PbI_2$ and MAAc. As illustrated in **Figure S2**, the new peaks at 141.8 eV and 137 eV in the Pb 4f XPS spectra and the peaks shift in the I 3d XPS spectra indicated the coordination between Pb and Ac as well as the

formation of the hydrogen bond between the MA and iodide. These results indicates that a second phase in the MAAc-$PbI_2$ film should be present. We assign this second phase to be $MAPbI_xAc_{3-x}$, which possesses a $MAPbI_3$-like tetragonal structure.[7c, 7d, 12]

The co-existence of $PbI_2$ and $MAPbI_xAc_{3-x}$ phases changes the film morphology. As reflected in the AFM images and calculated crystal sizes by Scherrer Equation (**Figure S3a, b** and **Table S1**), the MAAc-$PbI_2$ film shows a smoother surface with larger grain sizes and larger interplanar spacing in comparison with the neat $PbI_2$ film. The more-aligned crystal orientation, larger grain size, smoother surface and larger interplanar spacing of the MAAc-$PbI_2$ film will potentially facilitate the permeation of the organic FAI and MAI, leading to the formation of the perovskite crystals with good alignment, film morphology and higher crystallinity.[10]

Upon depositing the FAI/MAI/MACl mixture onto the $PbI_2$-based precursor film, smooth perovskite films with uniform grain sizes are formed with the aid of MAAc additive (**Figure S3c, d** and **Table S2**). Furthermore, the perovskite crystals with MAAc additive exhibit better alignment, especially in the (110) diffractions, which can be confirmed by the comparison between the GIWAXS patterns (**Figure S4a, b**) and the derived azimuthal pole figure (**Figure S4c**).

From SEM images presented in **Figure 3a, b**, we observe after the incorporation of MAAc additive, the presence of excess $PbI_2$ in the resultant perovskite layer. The corresponding XRD pattern (**Figure 3c**) also shows more intensified $PbI_2$ diffraction peaks. Previous research already demonstrate that the excess $PbI_2$ distributed at the perovskite grain boundaries can passivate the surface defects[13]. In addition to a more intense $PbI_2$ diffraction peak at 12.6°, a splitting of diffraction peak in the 2θ range of 24.3° to 25.0° occurs in the MAAc-assisted perovskite film (**Figure 3d**). The single diffraction peak splits into two, which can be assigned to (112) and (202)

planes of the perovskite crystal. This phenomenon becomes more evident in the second-order diffraction peaks, where (224) and (404) peaks can be clearly identified (**Figure 3e**).

To our knowledge, FA-based cubic perovskites rarely show (112) and (224) crystal planes in the XRD pattern.[14] The peak splitting is possibly correlated with the structural transitions and indicates the formation of a second perovskite-like phase.[15] Compared to the diffraction peaks of MAAc-assisted $PbI_2$ precursor, we induce that the (112) and (224) planes originate from the intermediate $MAPbI_xAc_{3-x}$ phase, indicating a phase segregation in the perovskite layer treated with MAAc.

However, it is widely known that both the MAAc and $MAPbI_xAc_{3-x}$ is thermally unstable, readily decomposing at temperatures exceeding 60℃.[7d, 9a, 12, 16] As shown in **Figure S5a**, the MAAc-$PbI_2$ complex powers were easily decomposed at temperature higher than 60℃ with the evaporation of MAAc. In **Figure S5b**, the similar decomposition of $MAPbI_xAc_{3-x}$ starts at about 60℃ and the other mass lost at nearly 150℃ refers to the evaporation of MAI. It is important to note that the perovskite samples tested in **Figure S5b** were prepared via immersing the intermediate $PbI_2$ and MAAc-$PbI_2$ powders into the FAI/MAI solution without thermal treatment. The Fourier Transform Infrared Spectroscopy (FTIR) spectrum further confirms the complete elimination of MAAc in the final perovskite films, in which the absorption peaks of $Ac^-$ at around 800 nm is shown in MAAc-$PbI_2$ complex but absent in the perovskite (**Figure S5c, d**).[17] According to these results, the (112) and (224) planes shown in **Figure 3** should be assigned to the $MAPbI_3$, instead of the rest $MAPbI_xAc_{3-x}$ intermediate template.

Based on these results, we propose that the intermediate $MAPbI_xAc_{3-x}$ is formed by the combination of $PbI_2$ and MAAc in the precursor solution, resulting in a thermal-unstable perovskite-like template in $PbI_2$ film with a preferential vertical orientation. Besides, with the aid of MAAc, the quality of $PbI_2$ films were optimized with better surface morphology and larger grain sizes. After subsequent deposition of the FAI/MAI mixture and thermal annealing at 150℃, the intermediate $MAPbI_xAc_{3-x}$ decomposes along with the volatilization of MAAc and transforms into the $PbI_2$ spreading at the grain boundaries or the final $(FAPbI_3)_x(MAPbI_3)_y$ perovskite with the supplementary MAI and FAI.

Owing to the ab-initio molecular dynamics (AIMD) simulations, the $MAPbI_xAc_{3-x}$ shows long-term stability at 330 K within 1000 fs (**Figure S6**). This result is in consistent with our suggestion about the formation of the $MAPbI_xAc_{3-x}$ template under low temperature thermal treatment. Furthermore, by the density functional theory (DFT) simulation, the $MAPbI_xAc_{3-x}$ is easy to change into the $MAPbI_3$ with supplementary iodide ions under higher temperature. **Table S3** exhibits the energy of each structure and the $E_{form}$ is calculated by the equation: $E_{form}=E(MAPbI_xAc_{3-x})- E(MAPbI_3)-E(Ac)$. The positive $E_{form}$=0.87 eV means that the transition from $MAPbI_xAc_{3-x}$ to $MAPbI_3$ is easy to happen, which is in accordance with experimental results and confirms that the $MAPbI_xAc_{3-x}$ formed and contributed to the growth of the final perovskite phase during the crystallization process.

The metastable intermediate $MAPbI_xAc_{3-x}$ affords a perovskite-like template, which ensures a regular and homogeneous crystal ordering with vertical alignment and prevents the formation of hexagonal phase (**Figure S7**).[3a, 18] This probably contributes to the highly crystalline perovskite

crystals with reduced defects densities and less recombination centers[19], resulting in prolonged carrier lifetime and efficient charge dynamics.

To verify the possible decrease of defect densities in perovskite film treated with MAAc, the space-charge-limited current (SCLC) measurement was carried out.[20] **Figure 4a, b** illustrate the dark *I-V* curves for electron-only devices (ITO/$SnO_2$/perovskite with and without MAAc/[6,6]-phenyl-C61-butyric acid methyl ester (PCBM)/Ag). Where three regions are observed: the Ohmic region at low bias exhibiting linear relation between current and electric field, the trap-filled limited region at intermediate bias region showing a sharp increase in current, and a trap-free SCLC region at high bias. The trap density levels are known to be continuously filled under the trap-filled limited transport region with increasing bias until saturation at the trap-filled limit voltage ($V_{TFL}$), extracted from the fitted dark *I-V* curves.[20b, 21] The trap density can be calculated using the equation of $N_t = 2(\varepsilon\varepsilon_0 V_{TFL})/(eL^2)$, where $\varepsilon$ is the dielectric constants of perovskite, $\varepsilon_0$ is the vacuum permittivity, $e$ is the elementary charge, and $L$ is the thickness of perovskite film.[22] The dielectric constant of the perovskite can be calculated according to $\varepsilon = (C_g L)/(\varepsilon_0 A)$, where $C_g$ is the geometrical capacitance of perovskite layer and the $A$ is the active areas of the electron-only device.[20b] $C_g$ is obtained by fitting the impedance spectra of device (ITO/perovskite with and without MAAc/Au) shown in **Figure S8.** All the parameters are listed in **Table S4**. Upon treating with MAAc, the estimated defect density in perovskite is reduced by an order of magnitude from $2.60\times10^{16}$ to $3.90\times10^{15}$ $cm^{-3}$, confirming that the MAAc additive can effectively passivate the perovskite defects.

In addition, steady-state photoluminescence (SSPL) and time-resolved photoluminescence (TRPL) were conducted to investigate the radiative recombination and carrier lifetime.[20b] PL

intensity decay curves are fitted using a bi-exponential decay equation of $I(t) = I_0 + A_1exp(-t/\tau_1) + A_2exp(-t/\tau_2)$, where $\tau_1$ and $\tau_2$ represent fast and slow decay time constant, respectively. Average time constant ($\tau_{ave}$) is calculated using relation of $\tau_{ave} = (A_1\tau_1^2 + A_2\tau_2^2)/(A_1\tau_1 + A_2\tau_2)$. As shown in **Figure 4c**, the steady-state PL intensity of the MAAc-assisted sample is higher than that of the control sample (light incident on perovskite side), suggesting suppressed radiative recombination in MAAc-assisted perovskite layer. Compared to the control sample, a slight blue shift of the excitation peak is observed in the MAAc additive sample, which may due to lower defect density at the band edge and the enhanced $PbI_2$ distribution.[23] The estimated carrier lifetime are 442 ns and 853 ns for the control and MAAc additive samples, respectively (**Figure 4d**). The significantly prolonged carrier lifetime in the MAAc-assisted perovskite film agrees well with its increased PL intensity. These results strongly suggest that MAAc additive can effectively passivate and reduce the defects through the considerable improvement in crystal ordering, ultimately yielding high $V_{OC}$ and FF in device. Besides, the obviously reduced PL intensity and lifetime in **Figure 4e, f** indicate an optimized electron extraction ability in the MAAc-assisted perovskite film, accounting for its greater FF value in device.

To further investigate the charge recombination kinetics in perovskite solar cells, photovoltage decay measurements at open circuit was conducted.[24] **Figure 4g** presents the results of transient photovoltage (TPV) measurements of ITO/$SnO_2$/perovskite/Spiro-OMeTAD/$MoO_3$/Ag devices with and without MAAc. The decay kinetics in control and MAAc-assisted devices can be well fitted with bi-exponential $V = I_0 + A_1exp(-t/\tau_1) + A_2exp(-t/\tau_2)$, which suggests two decay routes assigning to bimolecular and trap-assisted recombination.[25] The values of $\tau_1$ and $\tau_2$ under solar conditions are 44 ns/167 ns and 53 ns/229 ns for the control and MAAc additive devices,

respectively, indicating longer carrier lifetime under both decay routes. This is consistent with the results of faster charge extraction and reduced defects density mentioned above. In addition, the slopes obtained from the light intensity dependence of $V_{OC}$ are 1.50 $k_BT/q$ and 1.25 $k_BT/q$ for the control and MAAc-assisted devices, respectively, where $k_B$ is the Boltzmann constant, $T$ is temperature and $q$ is the electric charge (**Figure 4h**). This further confirms that non-radiative recombination routes arising from deep-level point defects were effectively suppressed in the device treated with MAAc additive.

To further verify the effect of this 'PPP' crystallization strategy, in addition to MAAc, GuaCl is applied to optimize the crystal growth either. Different from the low solubility and the MA cations in MAAc, GuaCl can dissolve in the $PbI_2$ precursor solution at relatively large concentrations, and has similar chemical structure and ion radius to the FA salts. Owing to this fact, GuaCl is introduced in 1.5 M precursor $PbI_2$ solution. As shown in the AFM images (**Figure S9**), the $PbI_2$ film with GuaCl is much smoother and more compact than the control. Moreover, the grain size in GuaCl-$PbI_2$ film is much larger than in the control film. The formed perovskite films with GuaCl additive showed the same tendency as well.

**Figure S10a** exhibited the XRD patterns of the $PbI_2$ film without and with GuaCl. GuaCl-$PbI_2$ film has an extra diffraction peak at 11.6° in addition to the signals from $PbI_2$. According to previous study [26], this new peak can be assigned to the GuaCl-$PbI_2$ 2D perovskite-like intermediate template, which was quite similar to the MAAc-$PbI_2$ complex that formed by hydrogen bond and coordination. After the formation of the perovskite, this GuaCl-$PbI_2$ intermediate 2D perovskite like template disappeared as shown in **Figure S10b**. With the aid of GuaCl-$PbI_2$, the formed perovskite showed much higher crystallinity with less $PbI_2$ left. **Table S5**

listed the interplanar spacing of $PbI_2$ and perovskite films with and without GuaCl calculated by Scherrer Equation. The increased interplanar spacing of $PbI_2$ and perovskite films with GuaCl was in accordance with the results in AFM images.

**Figure S10c** revealed the results of the TG test for the $PbI_2$ and GuaCl-$PbI_2$ complex powers. Similar to the MAAc-$PbI_2$, the GuaCl-$PbI_2$ intermediate phase starts to degrade at 80 ℃ with the decomposition of Gua cation, which turned to be the carbamide, in air condition. When the temperature is higher than 150 ℃, the degraded carbamide further decomposed into the ammonia gas and carbon dioxide. Thus, it was suggested that the GuaCl-$PbI_2$ intermediate phase was formed in the precursor $PbI_2$ films and decomposed during the high temperature annealing process of the perovskite, effecting in the same way as MAAc-$PbI_2$.

When incorporating the perovskite films with and without GuaCl additive to the solar cells, the $V_{oc}$ and FF increased from 1.12 V to 1.16 V and 76.2% to 79.4% in control and GuaCl based perovskite solar cells, respectively (**Figure S11** and **Table S6**). As a result, the PCE was increased from 21.2% to 22.8%, indicating a balanced charge transport, effective passivation of deep-level defects and reduced non-radiative recombination.

All these results proved that the 'PPP' growth strategy is an effective and universal method to suppress the formation of deep-level defects and non-radiative recombination in perovskite films, contributing to further development of the highly efficient PSCs and other perovskite-based optoelectronic devices.

**Conclusion**

In summary, a PPP growth strategy is demonstrated to effectively suppress the formation of deep-level defects in PSCs. The thermally-unstable perovskite-like intermediate phase enables the formation of highly crystalline perovskite layer with improved alignment. As a result, the deep-level trap states, which serve as recombination centers, are significantly suppressed in the formed perovskite films, resulting in simultaneously improved $V_{OC}$ and FF, and ultimately a superior PCE of 22.3% and 22.8% for MAAc-based and GuaCl-based devices. Overall, this work presents an effective approach to suppress the unhomogeneous crystallization and deep-level defects hindering the device PCE and stability, and therefore could contribute to the further development of highly efficient and large scale PSCs as well as other perovskite-based optoelectronic devices.

**Supporting Information**

Supporting Information is available from the Wiley Online Library or from the author.

**Acknowledgements**

This work was financially supported by research grants from the Natural Science Foundation of China (62074022, 12004057), the Natural Science Foundation of Chongqing (cstc2018jszx-cyzdX0137, cstc2020jcyj-msxmX0851), the Fundamental Research Funds for the Central Universities (2020CDJQY-A055, 2020CDJ-LHZZ-044) and the Key Laboratory of Low-grade Energy Utilization Technologies and Systems (LLEUTS-201901).

**Conflict of Interest**

The authors declare no conflict of interest.

**References**

[1] Q. Jiang, Y. Zhao, X. Zhang, X. Yang, Y. Chen, Z. Chu, Q. Ye, X. Li, Z. Yin, J. You, *Nat. Photonics* **2019**, 13, 460.

[2] a) S.-W. Lee, S. Bae, D. Kim, H.-S. Lee, *Adv. Mater.* **2020**; b) Y. Wang, Z. Zhang, M. Tao, Y. Lan, M. Li, Y. Tian, Y. Song, *Nanoscale* **2020**, 12, 18563.

[3] a) H. Yu, F. Wang, F. Xie, W. Li, J. Chen, N. Zhao, *Adv. Funct. Mater.* **2014**, 24, 7102; b) W. S. Yang, B.-W. Park, E. H. Jung, N. J. Jeon, Y. C. Kim, D. U. Lee, S. S. Shin, J. Seo, E. K. Kim, J. H. Noh, S. I. Seok, *Science* **2017**, 356, 1376.

[4] W. S. Yang, J. H. Noh, N. J. Jeon, Y. C. Kim, S. Ryu, J. Seo, S. I. Seok, *Science* **2015**, 348, 1234.

[5] J. Cao, X. Jing, J. Yan, C. Hu, R. Chen, J. Yin, J. Li, N. Zheng, *J. Am. Chem. Soc.* **2016**, 138, 9919.

[6] a) Q. L. Wu, P. C. Zhou, W. R. Zhou, X. F. Wei, T. Chen, S. F. Yang, *ACS Appl. Mater. Interfaces* **2016**, 8, 15333; b) D. Forgacs, M. Sessolo, H. J. Bolink, *J. Mater. Chem. A* **2015**, 3, 14121; c) C. Gao, H. Dong, X. Bao, Y. Zhang, A. Saparbaev, L. Yu, S. Wen, R. Yang, L. Dong, *J. Mater. Chem. C* **2018**, 6, 8234; d) Z. Liu, L. Wang, J. Han, F. Zeng, G. Liu, X. Xie, *Org. Electron.* **2020**, 78, 105552; e) C. Li, Z. Zhu, Y. Wang, Q. Guo, C. Wang, P. Zhong, Z. a. Tan, R. Yang, *Nano Energy* **2020**, 69, 104380.

[7] a) W. Zhang, M. Saliba, D. T. Moore, S. K. Pathak, M. T. Hoerantner, T. Stergiopoulos, S. D. Stranks, G. E. Eperon, J. A. Alexander-Webber, A. Abate, A. Sadhanala, S. Yao, Y. Chen, R. H. Friend, L. A. Estroff, U. Wiesner, H. J. Snaith, *Nat. Commun.* **2015**, 6, 6142; b) Y. Fu, F. Meng, M. B. Rowley, B. J. Thompson, M. J. Shearer, D. Ma, R. J. Hamers, J. C. Wright, S. Jin, *J. Am. Chem.*

*Soc.* **2015**, 137, 5810; c) L. C. Zhao, D. Y. Luo, J. Wu, Q. Hu, W. Zhang, K. Chen, T. H. Liu, Y. Liu, Y. F. Zhang, F. Liu, T. P. Russell, H. J. Snaith, R. Zhu, Q. H. Gong, *Adv. Funct. Mater.* **2016**, 26, 3508; d) Y. Zhang, Y. Ma, I. Shin, Y. K. Jung, B. R. Lee, S. Wu, J. H. Jeong, B. H. Lee, J. H. Kim, K. H. Kim, S. H. Park, *ACS Appl. Mater. Interfaces* **2020**, 12, 7186.

[8] A. K. Jena, A. Ishii, Z. Guo, M. A. Kamarudin, S. Hayase, T. Miyasaka, *ACS Appl. Mater. Interfaces* **2020**, 12, 33631.

[9] a) L. Chao, Y. Xia, B. Li, G. Xing, Y. Chen, W. Huang, *Chem* **2019**, 5, 995; b) D. Li, L. Chao, C. Chen, X. Ran, Y. Wang, T. Niu, S. Lv, H. Wu, Y. Xia, C. Ran, L. Song, S. Chen, Y. Chen, W. Huang, *Nano Lett.* **2020**, 20, 5799; c) J. Qiu, Y. Xia, Y. Chen, W. Huang, *Adv. Sci.* **2019**, 6, 1800793; d) X. Wang, X. Ran, X. Liu, H. Gu, S. Zuo, W. Hui, H. Lu, B. Sun, X. Gao, J. Zhang, Y. Xia, Y. Chen, W. Huang, *Angew. Chem. Int. Ed.* **2020**, 59, 13354; e) L. Chao, T. Niu, H. Gu, Y. Yang, Q. Wei, Y. Xia, W. Hui, S. Zuo, Z. Zhu, C. Pei, X. Li, J. Zhang, J. Fang, G. Xing, H. Li, X. Huang, X. Gao, C. Ran, L. Song, L. Fu, Y. Chen, W. Huang, *Research* **2020**, 2020, 1.

[10] Q. Jiang, Z. Chu, P. Wang, X. Yang, H. Liu, Y. Wang, Z. Yin, J. Wu, X. Zhang, J. You, *Adv. Mater.* **2017**, 29, 1703852.

[11] D. T. Moore, K. W. Tan, H. Sai, K. P. Barteau, U. Wiesner, L. A. Estroff, *Chem. Mat.* **2015**, 27, 3197.

[12] R. Fu, Y. Zhao, W. Zhou, Q. Li, Y. Zhao, Q. Zhao, *J. Mater. Chem. A* **2018**, 6, 14387.

[13] Y. Chen, Q. Meng, Y. Xiao, X. Zhang, J. Sun, C. B. Han, H. Gao, Y. Zhang, Y. Lu, H. Yan, *ACS Appl. Mater. Interfaces* **2019**, 11, 44101.

[14] a) Z. Li, M. J. Yang, J. S. Park, S. H. Wei, J. J. Berry, K. Zhu, *Chem. Mat.* **2016**, 28, 284; b) C. Y. Yi, J. S. Luo, S. Meloni, A. Boziki, N. Ashari-Astani, C. Gratzel, S. M. Zakeeruddin, U. Rothlisberger, M. Gratzel, *Energy Environ. Sci.* **2016**, 9, 656.

[15] a) L. J. Hu, K. Sun, M. Wang, W. Chen, B. Yang, J. H. Fu, Z. Xiong, X. Y. Li, X. S. Tang, Z. G. Zang, S. P. Zhang, L. D. Sun, M. Li, *ACS Appl. Mater. Interfaces* **2017**, 9, 43902; b) L. J. Hu, M. Li, K. Yang, Z. Xiong, B. Yang, M. Wang, X. S. Tang, Z. G. Zang, X. X. Liu, B. C. Li, Z. Y. Xiao, S. R. Lu, H. Gong, J. Y. Ouyang, K. Sun, *J. Mater. Chem. A* **2018**, 6, 16583.

[16] Y. Xiao, L. Yang, G. Han, Y. Li, M. Li, H. Li, *Org. Electron.* **2019**, 65, 201.

[17] Y. Xia, C. Ran, Y. Chen, Q. Li, N. Jiang, C. Li, Y. Pan, T. Li, J. Wang, W. Huang, *J. Mater. Chem. A* **2017**, 5, 3193.

[18] M. Qin, K. Tse, T.-K. Lau, Y. Li, C.-J. Su, G. Yang, J. Chen, J. Zhu, U. S. Jeng, G. Li, H. Chen, X. Lu, *Adv. Mater.* **2019**, 31, 1901284.

[19] Z.-K. Wang, M. Li, Y.-G. Yang, Y. Hu, H. Ma, X.-Y. Gao, L.-S. Liao, *Adv. Mater.* **2016**, 28, 6767.

[20] a) S. G. Kim, J. Chen, J. Y. Seo, D. H. Kang, N. G. Park, *ACS Appl. Mater. Interfaces* **2018**, 10, 25372; b) J. Chen, X. Zhao, S.-G. Kim, N.-G. Park, *Adv. Mater.* **2019**, 31, 1902902; c) V. V. Brus, A. K. K. Kyaw, P. D. Maryanchuk, J. Zhang, *Prog. Photovoltaics Res. Appl.* **2015**, 23, 1526.

[21] P. Kumar, S. C. Jain, V. Kumar, S. Chand, R. P. Tandon, *Eur. Phys. J. E* **2009**, 28, 361.

[22] a) J. Chen, J.-Y. Seo, N.-G. Park, *Adv. Energy Mater.* **2018**, 8, 1702714; b) J. Bisquert, L. Bertoluzzi, I. Mora-Sero, G. Garcia-Belmonte, *J. Phys. Chem. C* **2014**, 118, 18983; c) J. Chen, S.-G. Kim, N.-G. Park, *Adv. Mater.* **2018**, 30, 1801948; d) J. Chen, S.-G. Kim, X. Ren, H. S. Jung, N.-G. Park, *J. Mater. Chem. A* **2019**, 7, 4977.

[23] N. K. Noel, S. N. Habisreutinger, B. Wenger, Y.-H. Lin, F. Zhang, J. B. Patel, A. Kahn, M. B. Johnston, H. J. Snaith, *Adv. Energy Mater.* **2020**, 10, 1903231.

[24] a) H. Chen, D. Hu, Q. Yang, J. Gao, J. Fu, K. Yang, H. He, S. Chen, Z. Kan, T. Duan, C. Yang, J. Ouyang, Z. Xiao, K. Sun, S. Lu, *Joule* **2019**, 3, 3034; b) K. Yang, S. Chen, J. Fu, S. Jung, J. Ye, Z. Kan, C. Hu, C. Yang, Z. Xiao, S. Lu, K. Sun, *ACS Appl. Mater. Interfaces* **2020**, 12, 30954.

[25] D. Hu, Q. Yang, H. Chen, F. Wobben, V. M. Le Corre, R. Singh, T. Liu, R. Ma, H. Tang, L. J. A. Koster, T. Duan, H. Yan, Z. Kan, Z. Xiao, S. Lu, *Energy Environ. Sci.* **2020**, 13, 2134.

[26] F. J. Zhang, B. Cai, J. Z. Song, B. N. Han, B. S. Zhang, H. B. Zeng, *Adv. Funct. Mater.* **2020**, 30, 11.

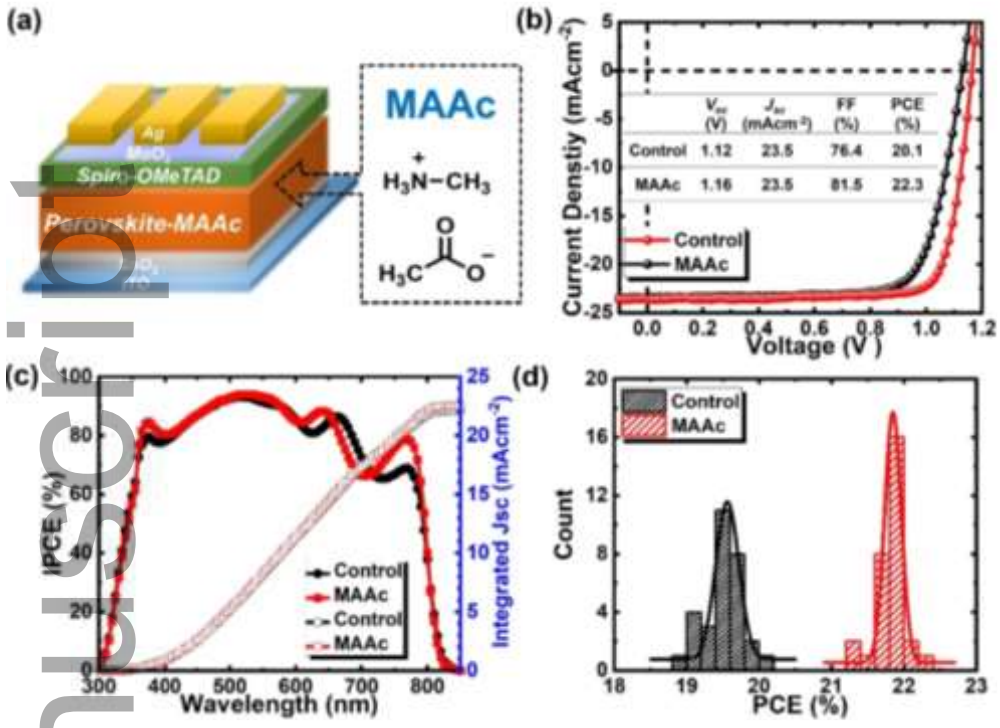


| | $V_{oc}$ (V) | $J_{sc}$ (mAcm$^{-2}$) | FF (%) | PCE (%) |
|---|---|---|---|---|
| Control | 1.12 | 23.5 | 76.4 | 20.1 |
| MAAc | 1.16 | 23.5 | 81.5 | 22.3 |

**Figure 1.** a) Schematic device structure adopted in this work and the chemical structure of methylamine acetate (MAAc). b) *J-V* curves and c) corresponding IPCE spectra of the optimal devices with and without MAAc additive measured under simulated AM 1.5G illumination. d) Statistical distribution of PCEs of PSCs based on the control and MAAc-doped devices for 40 devices.

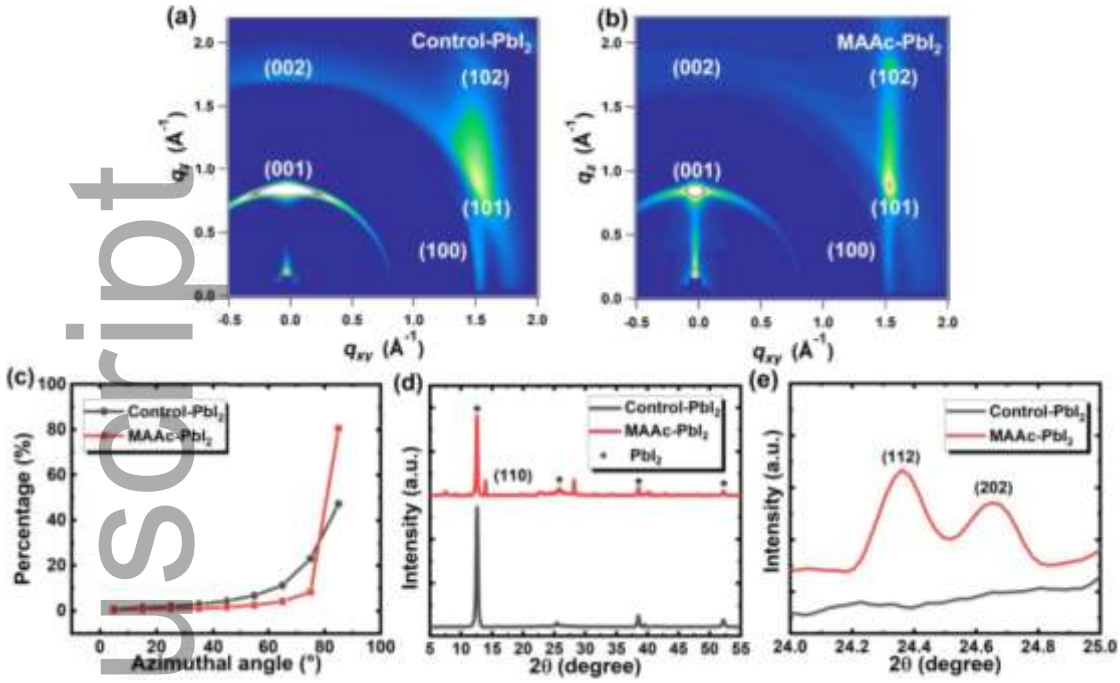


**Figure 2.** GIWAXS patterns of the $PbI_2$ films prepared a) without and b) with MAAc after annealing at 60℃ for 1 min. c) The intensity azimuthal pole figure of (001) diffractions of the $PbI_2$ films prepared without and with MAAc after annealing at 60℃ for 1 min. d) XRD diffraction pattern of the $PbI_2$ films prepared with and without MAAc after annealing at 60℃ for 5 min. e) Magnified image of XRD spectra in the range between 24.0° and 25.0°.

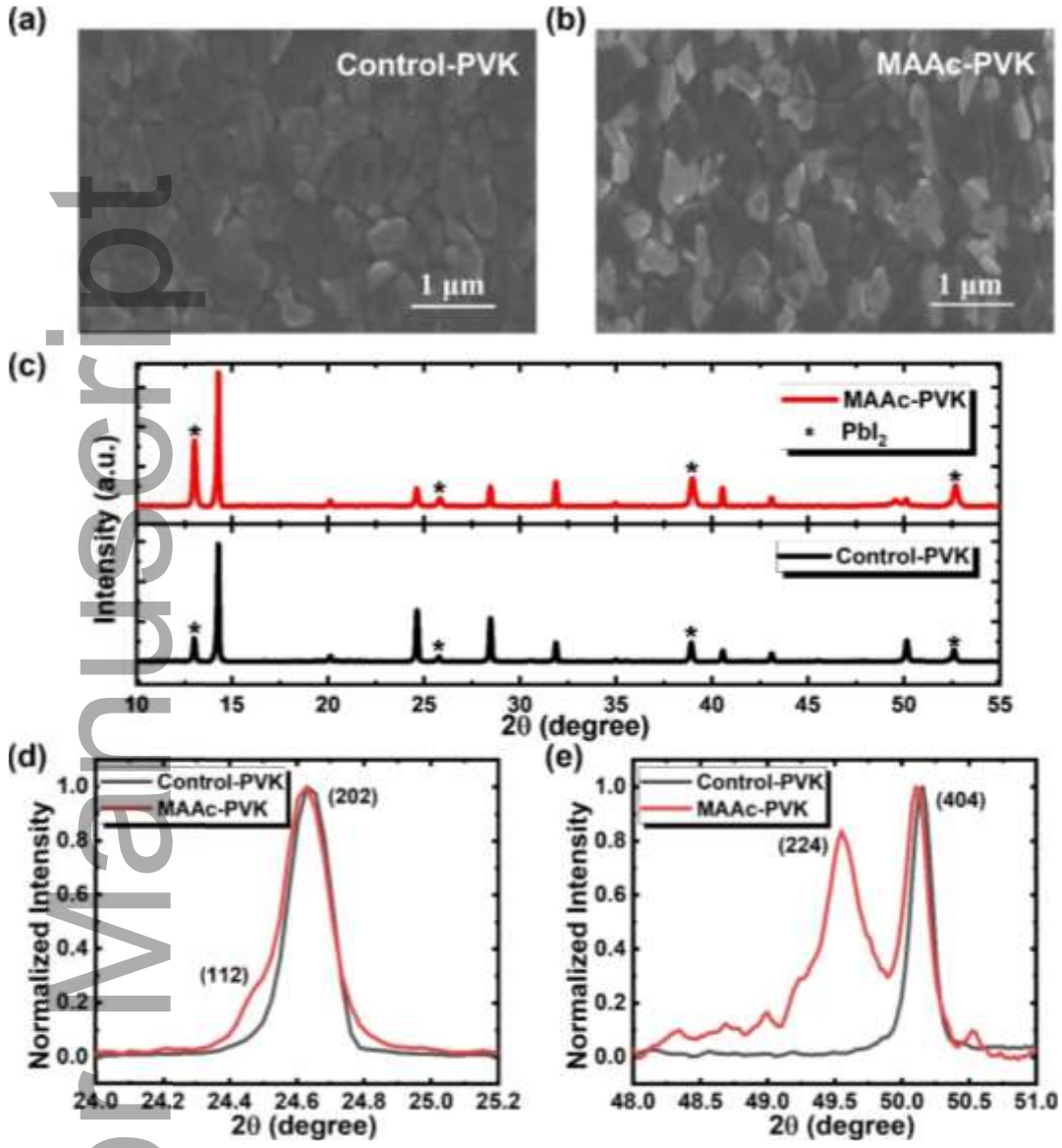


**Figure 3.** Top-view SEM images of perovskite films deposited a) without and b) with MAAc. c) XRD diffraction patterns of the perovskite films prepared with and without MAAc. d) and e) Magnified XRD spectra in the range of 24.0°-25.2° and 48.0°-51.0°, respectively.

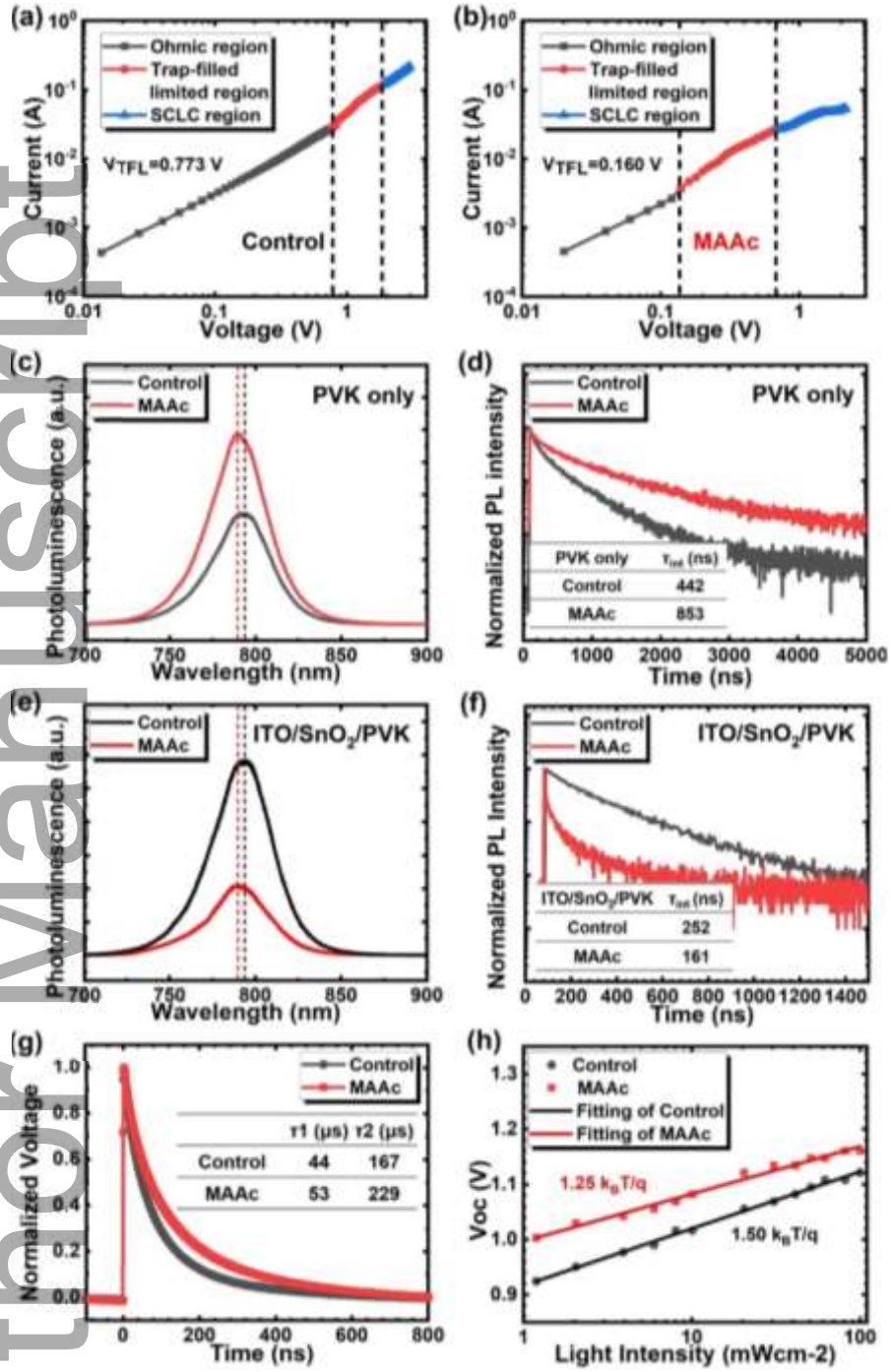


**Figure 4.** Dark *I-V* curves of electron-only devices with a cell architecture of ITO/$SnO_2$/perovskite a) without and b) with MAAc/PCBM/Ag. c) Steady-state photoluminescence (SSPL) and d) time-resolved photoluminescence (TRPL) spectra of perovskite films with and without MAAc. e) SSPL and f) TRPL spectra of perovskite films deposited on the $SnO_2$ and ITO substrate. g) Transient photovoltage based on devices with and without MAAc. (h) $V_{OC}$ versus light intensity plots of PSCs with and without MAAc.

**A 'Precursor to Perovskite-like template to Perovskite' (PPP) growth strategy** is used for the first time to control the phase transition and suppress the formation of deep-level defects during crystallization process. The defect density is reduced by an order of magnitude and the carrier lifetime is doubled in the highly orientated perovskite films, yielding impressive PCE of 22.3% and 22.8% in the devices. To the best of our knowledge, the PCE of 22.3% is the highest PCE using acetate anion in perovskite solar cells.

**Keywords**: perovskite solar cells, self-sacrificed template, crystal growth, deep-level defects, non-radiative recombination.

*Zhuang Xiong[a], Shanshan Chen[b], Pengjun Zhao[c], Yongjoon Cho[d], George Omololu Odunmbaku[a], Yujie Zheng[b], David J. Jones[c], Changduk Yang[d], Kuan Sun[a,]**

**Title: Phase Transition Modulation and Defects Suppression in Perovskite Solar Cells Enabled by a Self-sacrificed Template**

**ToC figure ((Please choose one size: 55 mm broad × 50 mm high or 110 mm broad × 20 mm high. Please do not use any other dimensions))**